Supplemental Information

EXTENDED EXPERIMENTAL PROCEDURES

Plasmids, Cell Lines, Antibodies, and Other Reagents

CHO cells stably expressing FR-GPI were maintained in Ham's F12 medium and imaged after labeling with a fluorescent analog of folic acid, PLB (pteroyl lysine conjugated to BODIPY-TMR) or PLF (pteroyl lysine conjugated to fluorescein) (Goswami et al., 2008). PSA3 cell lines were maintained in Ham's F12 medium in the presence of 10μM ethanolamine. PGAP2/3 double mutant cell lines (of CHO origin) stably expressing CD59 and DAF were maintained in Ham's F12 medium with Geniticin (600 μg/ml), puromycin (6 μg/ml) and blasticidin (6 μg/ml) as described in Maeda et al. (2007). FR-TM-Ez cell line was generated as described previously (Gowrishankar et al., 2012).

Alexa-conjugated 488 FLAER™ (A488F; Protox Biotech), Alexa 647 conjugated AnnexinV and F-DHPE (Invitrogen Inc), cDNA encoding Lact C2-GFP (Addgene), secondary antibodies (Jackson ImmunoResearch Laboratories, Inc), Jasplakinolide (Calbiochem) were purchased from the indicated sources. cDNA encoding Lact C2 Ez YFP was obtained from the Protein Technology Core at C-Camp (D.V. Koster, M. Neerathilingam, and S.M., unpublished data). Unless otherwise indicated all other reagents were obtained from Sigma. Mov18 antibody (Kumari and Mayor, 2008), BODIPY dye [6-{4,4-difluoro-1,3-dimethyl-5-(4-methoxyphenyl)-4-bora-3a,4a-diaza-s-indacene-2-propionyl}amino]-hexanoic acid-succinimidyl ester was procured from Invitrogen. DHPE was conjugated to Bodipy^{TMR} as described in Saikam et al., (2011). Synthetic PS lipids were purchased from Avanti polar lipids.

M1 (150 mM NaCl, 20 mM HEPES, 5 mM KCl, 1 mM $CaCl_2$ and 1 mM $MgCl_2$- pH 7.4) buffer was used for live imaging of cells with 1 mM Glucose (M1/Glc). Solvents for chemical synthesis were purified according to the standard procedures, and reagents used were of highest purity available. All reactions were performed in a flame-dried glass apparatus under argon/nitrogen atmosphere unless mentioned otherwise. Anhydrous solvents like CH_2Cl_2, Et_2O, THF, CH_3OH, CH_3CN, DMF, pyridine, Et_3N were freshly dried using standard methods. NMR measurements (^1H, ^{13}C and ^{31}P) were recorded on 200/400/500 MHz spectrometer (Bruker) fitted with pulse-field gradient probe, and tetramethylsilane (TMS) or residual resonance of deuterated solvent were used as internal reference. Chemical shifts are expressed in (δ) parts per million and coupling constants *J* in Hertz. Mass spectra were recorded on MALDI-TOF/TOF mass spectrophotometer using 2, 5-Dihydroxy benzoic acid/α-Cyano-4-hydroxy cinnamic acid (Sigma-Aldrich) as matrix in acetonitrile: water containing 0.01% TFA. Optical rotations were measured on a digital PerkinElmer-241 polarimeter. For HPLC, LC 1100 (Agilent Technologies) instrument equipped with a binary pump was used. The samples were analyzed on a RP-18 column (Agilent, 5μm, 4.6 × 250 mm) using an eluent [water: acetonitrile (isocratic)] with flow rate 0.8 ml/min, at the temperature of 30°C and detector wavelength 544 nm. Analytical TLC was performed on Merck 60 F_{254} plates, and compounds were visualized by spraying and charring with phosphomolybdic acid or 20% H_2SO_4 in MeOH as developing reagent. Preparative TLC was performed on pre-coated silica gel 60 F_{254} plates (20x20 cm) purchased from Merck. Silica column chromatography was carried out with silica gel (100–200 mesh) or flash silica gel (230–400 mesh) purchased from Merck. The BODIPY dye [6-{4,4-difluoro-1,3-dimethyl-5-(4-methoxyphenyl)-4-bora-3a,4a-diaza-s-indacene-2-propionyl}amino]-hexanoic acid-succinimidyl ester was procured from Invitrogen. DHPE was conjugated to Bodipy^{TMR} as described in Saikam et al. (2011) and purified on preparative thin layer chromatography and confirmed by mass spectrometry.

Constructs and cell lines and their sources are listed in the table below:

Plasmid/ Cell line	Description	Source
PH-GFP	PH domain of PLCδ fused to GFP	Tobias Meyer (Stanford University)
C term Ez GFP	Actin binding c terminal domain of Ez fused to GFP	Antonio S Sechi (RWTH Aachen University, Germany)
PGAP2/3 cell line	PGAP2/3 double mutant cell line stably expressing CD59 and DAF	Taroh Kinoshita (Osaka University, Japan)
PSA3 cell line	Ethanolamine auxotroph which lacks PS synthase 1 enzyme	Tomohiko Taguchi (University of Tokyo, Japan)

GPI Analogs

The synthesis of fluorescently tagged GPI analogs $GPI_{C16:0/C16:0}$ was carried out as reported by deprotection of *tert*-butyloxycarbonyl (BOC)-derivatives of GPI analogs followed by labeling with BODIPY (Saikam et al., 2011). The same synthetic strategy was adopted for the synthesis of $GPI_{C8:0/C8:0}$ and the data provided as below.

(6-Amino-6-deoxy-2-*N*-(*tert*-butyloxycarbonyl)-amino-2-deoxy-α-D-glucopyranosyl)-(1–6)-1-*O*-[(1,2-dioctanoyl)-*sn*-glycery-phosphonato-D-*myo*-inositol (GlcN(BOC)$PI_{C8:0/C8:0}$)

(yield, 80%). $[\alpha]_D$ = +12.34 (c 0.01, $CHCl_3$); ^1H NMR (500 MHz, $CDCl_3$): δ 5.52 (brs, 1H), 5.25 (brs, 1H), 5.18-5.17 (d, *J* = 3.21, 1H), 4.42-4.40 (m, 1H), 4.30-4.21 (m, 2H), 4.07-4.05 (m, 2H), 3.85-3.82 (m, 1H), 3.65-3.61 (m, 3H), 3.34-3.30 (m, 4H), 3.21-3.19 (q, *J* = 7.3, 6H), 3.14-3.06 (m, 2H), 2.36-2.31 (m, 4H), 1.59-1.54 (m, 4H), 1.45-1.44 (t, *J* = 6.6, 9H), 1.33-1.22 (m, 25H), 0.91-0.86 (t, *J* = 7.0, 6H); MALDI TOF MS: calculated for $C_{36}H_{66}N_2O_{18}P$ $(M+H)^+$ 846.4126, found 846.4252.

[2-Amino-2-deoxy-6-*N*-(BODIPY)-amino-6-deoxy-α-D-glucopyranosyl]-*myo*-D-inositol-1-[*sn*-2,3-bis(octanoyloxy) propyl phosphate] ($GPI_{C8:0/C8:0}$)

TLC {EtOAc:$(Me)_2CO$:MeOH:H_2O (7:1:1:1)} as eluent to give ($GPI_{C8:0/C8:0}$) (yield, 62%). ^{31}P NMR (161 MHz, CD_3OD, $CDCl_3$): δ −1.35; MALDI TOF MS: calculated for $C_{58}H_{89}BF_2N_5O_{19}P$ $(M+H-F)^+$ 1240.6029, found 1240.6043.

The GPI analogs with fluorescein labels and lipid tails of varying degrees of saturation ($GPI_{C18:0/C18:0}$ and $GPI_{C18:1/C18:1}$) were synthesized as described previously (Johnson and Guo, 2013).

PS Analogs

Synthetic PhospholipaseA2-susceptible PS lipids were purchased from Avanti polar lipids. The synthetic strategy of PLA_2-resistant PS analogs and the characterization data for the same is given below:

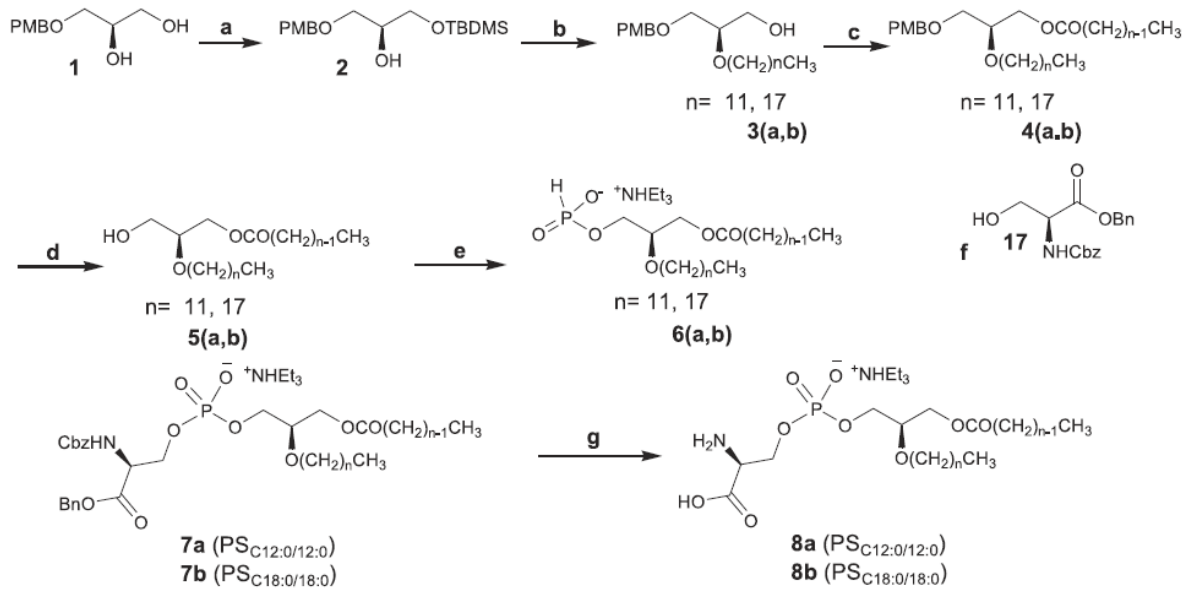

Reagents and Conditions

(a) TBDMS chloride, imidazole,CH_2Cl_2, 10 hr, 82% (b) i) $CH_3(CH_2)_nBr$, Bu4NI, DMF, THF, 2 h; ii). Bu_4NF, THF, 2 hr, 75% over two steps; (c) $CH_3(CH_2)_{n-1}COOH$, DCC, DMAP, CH_2Cl_2, 12 hr, 92%; (d) DDQ, CH_2Cl_2, H_2O, 2 hr, 55%; (e)PCl_3, imidazole, CH_2Cl_2, TEA, 3 hr, 90%; (f) pivaloyl chloride, dry pyridine, dry ACN, 1 hr and then I_2, pyridine, water, 2 hr, 92%; (g) $Pd(OH)_2$, H_2, CH_2Cl_2: MeOH: H_20, 18 hr, 82%.

(2S)-1-*O*-*tert*-butyldimethylsilyl-3-*O*-(4-methoxybenzyl)propanol (2)

To a solution of 3-(*p*-methoxybenzyl)-*sn*-glycerol **1** (1.62 g, 7.64 mmol) in 20 ml of CH_2Cl_2 was added TBDMSCl (1.203 g, 8.023 mmol) followed by imidazole (1.04 g, 15.29 mmol). The mixture was stirred at room temperature for 1 hr. The mixture was filtered and the filtrate was rinsed with 20 ml CH_2Cl_2. The solution was then extracted with H_2O (40 ml × 2). The organic layer was concentrated and purified by column chromatography on silica gel (eluting with EtOAc-Hexane 2:8) to afford 2.31 g (92%) of compound **2** as colorless syrup: R_f (SiO_2, EtOAc/Hexane 3:7) = 0.49; ^1H NMR (400 MHz, $CDCl_3$): δ 7.25 (d, *J* = 8.4 Hz, 2H), 6.88 (d, *J* = 8.5 Hz, 2H), 4.48 (s, 2H), 3.91 – 3.73 (m, 4H), 3.73 – 3.59 (m, 2H), 3.59 – 3.41 (m, 2H), 0.89 (s, 9H), 0.06 (s, 6H); HRMS (MALDI): calculated for $C_{17}H_{30}O_4Si$ $(M+Na)^+$ was found to be 349.1820.

(2R)-2-*O*-dodecyl-3-*O*-(4-methoxybenzyl)propanol (3a)

The substrate **2** (700 mg, 2.147 mmol) and *n*- Dodecyl bromide (1068 mg, 4.29 mmol) was dissolved in mixture of solvents DMF and THF (10 ml, 1:1). To this 257 mg (10.73 mmol) NaH (60% in mineral oil) and 10 mg of Bu4NI was added simultaneously at 0°C and stirred 8h at room temperature. MeOH (2 ml) was added to neutralize the excess of sodium hydride, diluted with EtOAc and washed with water and brine solution. The organic layer was dried over Na_2SO_4 and concentrated in vacuum. To a solution of the above crude product was added 6 ml of Bu_4NF (a 1 M solution in THF). After the mixture was stirred at rt(room temperature) for 4h, and then concentrated, the residue was treated with water and extracted with EtOAc (30 ml × 3). The organic layer was dried over Na_2SO_4. After concentration, 527 mg of **3a** (82% for two steps) was obtained a colorless liquid after purification by chromatography on silica gel (elution with 15:85 EtOAc/Hexane). ^1H NMR (400 MHz, $CDCl_3$) δ 7.24 (d, *J* = 8.5 Hz, 2H), 6.87 (d, *J* = 8.5 Hz, 2H), 4.47

(s, J = 12.5 Hz, 2H), 3.79 (s, 3H), 3.75 – 3.68 (m, 1H), 3.66 – 3.57 (m, 2H), 3.57 – 3.47 (m, 4H), 1.63 – 1.49 (m, 2H), 1.38 – 1.16 (m, J = 19.0 Hz, 18H), 0.88 (t, J = 6.7 Hz, 3H). HRMS (MALDI): calculated for $C_{23}H_{40}O_4$ $(M+Na)^+$ 403.2824 found 403.2816.

(2R)-2-*O*-octadecanyl-3-*O*-(4-methoxybenzyl)propanol (3b)

An identical procedure starting from the compound **2** and *n*-Octadecyl bromide gave **3b** (yield, 82%). ^{1}H NMR (400 MHz, $CDCl_3$) δ 7.24 (d, J = 8.5 Hz, 2H), 6.87 (d, J = 8.5 Hz, 2H), 4.47 (s, J = 12.5 Hz, 2H), 3.79 (s, 3H), 3.75 – 3.68 (m, 1H), 3.66 – 3.57 (m, 2H), 3.57 – 3.47 (m, 4H), 1.63 – 1.49 (m, 2H), 1.38 – 1.16 (m, J = 19.0 Hz, 30H), 0.88 (t, J = 6.7 Hz, 3H). HRMS (MALDI): calculated for $C_{29}H_{52}O_4$ $(M+Na)^+$ 487.3763 found 487.3743.

(2S)-2-*O*-dodecyl-3-*O*-(4-methoxybenzyl)propyl dodecanoate (4a)

To the stirred solution of free hydroxyl glycerol **3a** (528 mg, 1.29 mmol) in CH_2CH_2 (10 ml) was added lauric acid (193 μL, 1.54 mmol), DCC (397 mg, 1.93 mmol) and DMAP (235 mg, 1.93 mmol). After 12h the precipitate in the reaction mixture was filtered, concentrated in vacuum and purified by column chromatography to obtain compound **4a** (yield, 85%).^{1}H NMR (400 MHz, $CDCl_3$) δ 7.25 (d, J = 8.9 Hz, 2H), 6.87 (d, J = 8.5 Hz, 2H), 4.48 (s, 2H), 4.23 (dd, J = 11.6, 4.2 Hz, 1H), 4.11 (dd, J = 11.6, 5.7 Hz, 1H), 3.80 (s, 3H), 3.71 – 3.59 (m, 1H), 3.59 – 3.45 (m, 4H), 2.31 (dt, J = 15.1, 7.6 Hz, 2H), 1.79 – 1.46 (m, 4H), 1.44 – 1.14 (m, 34H), 0.96 – 0.77 (m, 6H). HRMS (MALDI): calculated for $C_{35}H_{62}O_5$ $(M+Na)^+$ 585.4495 was found to be 585.45.

(2S)-2-*O*-octadecanyl-3-*O*-(4-methoxybenzyl)propyl octadecanoate (4b)

In identical procedure starting from the compound **3b** and stearic acid gave **4b** (yield, 80%). ^{1}H NMR (400 MHz, $CDCl_3$) δ 7.25 (d, J = 8.8 Hz, 2H), 6.87 (d, J = 8.5 Hz, 2H), 4.47 (d, J = 6.1 Hz, 2H), 4.31 – 4.19 (m, 1H), 4.11 (dd, J = 11.6, 5.7 Hz, 1H), 3.80 (s, 3H), 3.69 – 3.58 (m, 1H), 3.58 – 3.39 (m, 4H), 2.31 (dt, J = 15.0, 7.6 Hz, 2H), 1.55 (ddd, J = 50.4, 25.3, 18.4 Hz, 4H), 1.27 (d, J = 2.7 Hz, 58H), 0.88 (t, J = 6.5 Hz, 6H). HRMS (MALDI): calculated for $C_{47}H_{86}O_5$ $(M+Na)^+$ 753.6373 found 753.6376.

2-*O*-dodecyl-1-*O*-dodecanyl-*sn*-glycerol (5a)

The above PMB protected glycerol intermediate **4a** (0.62 g, 1.59 mmol) was dissolved in CH_2Cl_2-H_2O (50 ml, 99:1) and treated with DDQ (750 mg) and the mixture stirred at room temperature overnight, diluted with CH_2Cl_2 (100 ml), washed three times with 10% $NaHCO_3$ solution. The organic layer was concentrated and the residue purified on a silica column to provide the desired compound (yield, 91%). ^{1}H NMR (400 MHz, $CDCl_3$) δ 4.27 – 4.07 (m, 2H), 3.80 – 3.39 (m, 5H), 2.37 (dt, J = 15.1, 7.8 Hz, 2H), 1.61 (ddd, J = 21.4, 14.5, 6.9 Hz, 4H), 1.28 (s, 38H), 0.90 (t, J = 6.8 Hz, 6H). HRMS (MALDI): calculated for $C_{27}H_{54}O_4$ $(M+Na)^+$ 465.392 found 465.3928.

2-*O*-octadecanyl-1-*O*-octadecanoyl-*sn*-glycerol (5b)

An identical procedure starting from the compound **4b** gave **5b** (yield, 92%). ^{1}H NMR (400 MHz, $CDCl_3$) δ 4.19 (d, J = 4.8 Hz, 2H), 3.77 – 3.41 (m, 5H), 2.35 (dd, J = 15.4, 7.9 Hz, 2H), 1.79 – 1.52 (m, 4H), 1.42 – 1.17 (m, 58H), 0.90 (t, J = 6.8 Hz, 6H). HRMS (MALDI): calculated for $C_{39}H_{78}O_4$ $(M+Na)^+$ 633.5798 found 633.578.

Triethylammonium 2-*O*-dodecanyl-1-*O*-dodecanoyl-*sn*-glycero-3-H-phosphonate (6a)

To a stirred solution of imidazole (42.5 mg, 0.61 mmol, dried through toluene evaporation) in anhydrous CH_2Cl_2 (0.5 ml) at 0°C was added PCl_3 (12 μL, 0.135 mmol dissolved in 125 μl CH_2Cl_2) followed by anhydrous triethyamine (48 μl, 0.35 mmol dissolved in 125 μl CH_2Cl_2). The stirring was continued for 10 min at 0°C and the temperature was lowered to –5°C and then a solution of **5a** (44 μmol dissolved in 0.5 ml CH_2Cl_2) was added dropwise. The reaction was stirred at –5°C for 2 hr and then quenched with pyridine-water (2.5 ml, 4:1) and stirred further for 30 min. This was followed by addition of $CHCl_3$ (7.5 ml), washing with H_2O (2.5 ml x 3). The $CHCl_3$ layer was dried (Na_2SO_4), concentrated and the residue purified through a silica column (1% MeOH-CH_2Cl_2 to 10% MeOH-CH_2Cl_2 with 1% TEA) to provide the desired lipid H-phosphonate donor **6a** (yield, 92%). ^{1}H NMR (400 MHz, $CDCl_3$) δ 7.72 (d, J = 27.9 Hz, 0.5H), 6.21 (d, J = 30.2 Hz, 0.5H), 4.34 – 4.20 (m, 1H), 4.20 – 4.07 (m, 1H), 3.96 (dt, J = 31.7, 15.9 Hz, 2H), 3.66 (ddd, J = 19.0, 9.7, 3.9 Hz, 1H), 3.61 – 3.47 (m, 2H), 2.33 (dt, J = 15.0, 9.4 Hz, 2H), 1.68 – 1.46 (m, 4H), 1.38 – 1.12 (m, 34H), 0.87 (dd, J = 7.5, 6.2 Hz, 6H). HRMS (MALDI): calculated for $C_{27}H_{54}O_6P$ $(M)^-$ 505.3663 found 505.3655.

Triethylammonium 2-*O*-octadecanyl-1-*O*-octadecanoyl-*sn*-glycero-3-H-phosphonate (6b)

An identical procedure starting from the compound **5b** gave **6b** (yield, 92%). ^{1}H NMR (400 MHz, $CDCl_3$) δ 7.73 (s, 0.5H), 6.16 (s, 0.5H), 4.27 (d, J = 7.6 Hz, 1H), 4.22 – 4.07 (m, 1H), 3.93 (d, J = 27.8 Hz, 2H), 3.69 (s, 1H), 3.56 (dd, J = 17.6, 7.4 Hz, 2H), 2.42 – 2.22 (m, 2H), 1.75 – 1.47 (m, 4H), 1.47 – 1.08 (m, 58H), 0.88 (t, J = 6.0 Hz, 6H). HRMS (MALDI): calculated for $C_{39}H_{78}O_6P$ $(M)^-$ 673.5542 found 673.5567.

Triethylammonium *O*-[(S)-2-(benzyloxycarbonyl)-2-(benzyloxycarbonylamino)ethyl]-*O*-(2-*O*-dodecyl-1-*O*-dodecanoyl-*sn*-glycero) phosphate 7a ($PS_{C12:0/C12:0}$*)

Freshly prepared H-phosphonate **6a** (18 mg, 0.04 mmol) and the serine intermediate (20 mg, 0.06 mmol, 1.3 equiv) were dried by evaporation with anhydrous pyridine three times, and dissolved in anhydrous pyridine (0.4 ml). This was followed by addition of pivaloyl chloride (2 equiv, 9.6 μL, 0.08 mmol). After stirring at room temperature for 30 min, the reaction was treated with an iodine

solution (2 equiv, 20 mg iodine in pyridine-water, 2.45:0.05) and the mixture was further stirred for 25 min. The reaction was diluted with $CHCl_3$ (12 ml) and the organic layer washed with a 5% sodium bisulfite solution (10 ml). The organic layer was dried over Na_2SO_4, concentrated and purified on a silica column using 5% MeOH-CH_2Cl_2 (with 1% triethylamine) solvent system, providing the desired phospho-coupled compound **7a** (yield, 88%). ^{1}H NMR (400 MHz, $CDCl_3$) δ 7.44 – 7.22 (m, 10H), 5.25 – 5.01 (m, 4H), 4.54 – 4.43 (m, 1H), 4.43 – 4.17 (m, 3H), 4.17 – 4.02 (m, 1H), 3.91 (dt, *J* = 11.7, 5.8 Hz, 2H), 3.76 – 3.60 (m, 1H), 3.60 – 3.42 (m, 2H), 2.37 – 2.21 (m, 2H), 1.67 – 1.46 (m, 4H), 1.43 – 1.08 (m, 34H), 0.90 (dt, *J* = 9.0, 7.4 Hz, 6H). HRMS (MALDI): calculated for $C_{44}H_{71}NO_{11}P$ $(M)^-$ 820.477 found 820.4758.

Triethylammonium *O*-[(S)-2-(benzyloxycarbonyl)-2-(benzyloxycarbonylamino)ethyl]-*O*-(2-*O*-octadecyl-1-*O*-octadecanoyl-*sn*-glycero) phosphate 7b ($PS_{C18:0/C18:0}$*)

An identical procedure starting from the compound **6b** gave **7b** (yield, 92%). ^{1}H NMR (400 MHz, $CDCl_3$) δ 7.47 – 7.16 (m, 10H), 5.28 – 4.99 (m, 4H), 4.53 – 4.40 (m, 1H), 4.39 – 4.16 (m, 3H), 4.16 – 3.99 (m,1H), 3.99 – 3.81 (m, 8H), 3.65 (qt, *J* = 10.9, 5.5 Hz, 1H), 3.59 – 3.39 (m, 2H), 2.29 (dd, *J* = 15.5, 8.0 Hz, 4H), 1.52 (ddd, *J* = 28.4, 17.6, 6.6 Hz, 4H), 1.38 – 1.10 (m, 58H), 0.95 – 0.78 (m, 6H). HRMS (MALDI): calculated for $C_{56}H_{95}NO_{11}P$ $(M)^-$ 988.6648 found 988.6667.

Triethylammonium 2-*O*-dodecyl-1-*O*-dodecanoyl-*sn*-glycero-3-phosphoserine 8a ($PS_{C12:0/C12:0}$*)

The protected PS intermediate **7a** (0.03 mmol) and the catalyst 20% $Pd(OH)_2$ (40 mg) were dissolved in a solvent mixture of MeOH (2 ml), CH_2Cl_2 (2 ml) and H_2O (0.05 ml). The residual and dissolved air from the flask was removed by repeated evacuations and the reaction mixture was stirred under hydrogen atmosphere overnight. After completion of the reaction, the mixture was filtered through a small celite pad, and concentrated under reduced pressure. The product was purified by a quick filtration through a silica column using MeOH-CH_2Cl_2 (1:1) to provide compound **8a ($PS_{C12:0/C12:0}$)** (yield, 81%).^{1}H NMR (400 MHz, $CDCl_3$) δ 4.40 – 4.19 (m, 2H), 4.10 (dd, *J* = 11.5, 6.2 Hz, 1H), 4.01 – 3.79 (m, 2H), 3.74 – 3.38 (m, 3H), 3.09 (s, 2H), 2.31 (t, *J* = 7.5 Hz, 2H), 1.67 – 1.56 (m, 4H), 1.52 (d, *J* = 6.3 Hz, 2H), 1.41 – 1.16 (m, 34H), 0.88 (q, *J* = 6.4 Hz, 6H). HRMS (MALDI): calculated for $C_{30}H_{59}NO_9P$ $(M)^-$ 608.3933 found 608.3908.

Triethylammonium 2-*O*-octadecyl-1-*O*-octadecanoyl-*sn*-glycero-3-phosphoserine 8b ($PS_{C18:0/C18:0}$*)

An identical procedure starting from the compound **7b** gave **8b ($PS_{C18:0/C18:0}$)** (yield, 82%).^{1}H NMR (400 MHz, $CDCl_3$) δ 4.42 – 4.19 (m, 2H), 4.10 (dd, *J* = 11.5, 6.2 Hz, 1H), 4.01 – 3.79 (m, 2H), 3.74 – 3.38 (m, 3H), 3.09 (s, 2H), 2.31 (t, *J* = 7.5 Hz, 2H), 1.66 – 1.56 (m, 4H), 1.52 (d, *J* = 6.3 Hz, 2H), 1.41 – 1.16 (m, 58H), 0.88 (q, *J* = 6.4 Hz, 6H). HRMS (MALDI): calculated for $C_{42}H_{83}NO_9P$ $(M)^-$ 776.5811 found 776.5825.

Triethylammonium 2-*O*-octadecene-yl-1-*O*-octadecenoyl-*sn*-glycero-3-phosphoserine ($PS_{C18:1/C18:1}$*)

Product was synthesized as described in (Bandyopadhyay and Bong, 2011). ^{1}HNMR (500 MHz, $CDCl_3$:CD_3OD:D_2O 8:2:0.1) δ 5.21-5.19 (t,3H), 4.25-3.91 (m, 10H), 2.17-2.14 (t,2H), 1.79-1.77(t,8H), 1.44-1.42 (t,2H), 1.37-1.35 (d,2H), 1.13-1.09 (t,40H), 0.71-0.69 (t,6H). HRMS (MALDI): calculated for $C_{42}H_{81}NO_9P$ 772.55 and found $(M+H)^+$ 775.2, $(M+Na)^+$ 797.2.

GPI Analog Incorporation

GPI analogs are incorporated into cell membranes by γ–CD method as described (Koivusalo et al., 2007). Briefly cells were incubated with lipid γ-CD complexes for 30 min at 37°C followed by replating cells onto fibronectin coated dishes to get rid of lipid sticking on the coverslip. During the process of replating at 37°C, some fraction of the GPI lipids at the plasma membrane was internalized into endosomes. These structures were identified by their co-localization with co-internalized dextran, or alternatively by their distinct punctate appearance, and were excluded from the anisotropy measurements.

PS Analog Incorporation and Endogenous GPI-AP Labeling

PS analogs were incorporated by Lipofectamine method as described (Saha et al., 2015) into PS depleted cells. The different PS analogs were incorporated to a similar extent as confirmed by AnnexinV labeling post ionomycin treatment as detailed below, followed by flow cytometry analysis (Figure S5C). PS depletion was carried out 48 hr prior to the experiment by incubating the cells at 37°C in medium containing dialysed serum. The cells were incubated with PS-lipofectamine complexes for 45 min at 10°C, washed with M1 buffer, followed by incubation at 37°C for 45 min in the presence or absence of PLA_2 inhibitor as indicated. The cells were then shifted to 4°C and endogenous GPI-APs at the plasma membrane were marked with Alexa 488 FLAER™ for 1 hr and imaged live.

DHPE Incorporation

B-DHPE was incorporated by making a complex with 1.5 mg/ml of BSA and F-DHPE with 10 mM γ-CD in incomplete medium without serum. The cells were incubated with serum free media for 30 min at 37° C after which they were labeled with DHPE-BSA complex for 30 min at 37°C, washed with serum containing medium to reduce sticking, then with M1 buffer and imaged live.

Assay for Determining whether Lipids Are Clustered

To test if the lipids are in nanoscale clusters, photobleaching followed by monitoring the change in homo-FRET provides a convenient method. On photobleaching, the molecules that are undergoing FRET in a cluster are turned off as a result of

which the measured anisotropy increases until all the FRET pairs are lost (Sharma et al., 2004). Briefly, cells labeled with PLB or incorporated with GPI analogs were continuously exposed to laser light and images were acquired at regular intervals, subsequently emission anisotropy was determined as a function of the extent of photobleaching with respect to initial intensity.

FCS/FRAP Measurements

Fluorescence correlation spectroscopy (FCS) measurements were performed as described previously (Gowrishankar et al., 2012). The fit of the autocorrelation curve was obtained by the Maximum Entropy Method (MEM), as described (Sengupta et al., 2002). For the Fluorescence recovery after photobleaching (FRAP) measurements, an LSM 5 Live confocal microscope (Ziess GMBH) equipped with line scanning capabilities, a SIM scanner and high NA objective (63X, 1.4 NA) were used. Briefly cells labeled with PLB or incorporated with GPI analogs were bleached at a single spot (14 μm size) and the measured recovery of fluorescence was fit to a single exponential fit $y = A(1 - e^{-xB})$. From the fit, the half time of diffusion, $t_{1/2} = -log(0.5)/B$ and mobile fraction, A was calculated. As a reference, 5 frames prior to photobleaching were acquired. For photobleaching correction, a spot away from the photobleached spot in the same cell was chosen.

Anisotropy Measurements

Steady state Homo-FRET based anisotropy measurements were carried out on a NikonTE2000 epifluorescence microscope with a dual camera imaging arrangement as described (Ghosh et al., 2012). On a wide-field set up, low resolution images were acquired with a 20X 0.7NA objective and high resolution images were acquired using a 100X 1.0 NA objective. Anisotropy is calculated by the formula

$$r = (Ipa - Ipe)/(Ipa + 2Ipe)$$

where Ipa is the intensity measured in the parallel direction and Ipe the intensity in the perpendicular direction with respect to the plane of polarization of the excitation beam. For measurements at low magnification and NA, the average anisotropy of each cell is measured. For high resolution images, 1x1 μm regions on the membrane excluding endosomes identified as described above, were selected by using Matlab routine and the anisotropy for each region was calculated.

Confocal based anisotropy measurements were acquired on a custom-designed NikonTiE epifluorescence microscope coupled to a spinning disc unit (Yokogawa CSU-22 scan head) as described (Ghosh et al., 2012). Briefly, a set of multi-wavelength (405, 488, 561, 633) polarized lasers input was used to excite the sample through a spinning disc unit and the emission path is identical to the wide field modality explained above except that emission light was split into Ipa and Ipe polarized light by means of a high- performance wire grid polarizer (Moxtek) and then collected onto two EMCCD cameras (Andor Ixon + 897) using an Andor TuCam dual camera adaptor. A 100X 1.4NA objective was used for imaging.

Antibody Crosslinking Experiments

Blebs were generated from CHO cells stably expressing FR-GPI or FR-TM-Ez by treating with 15uM Jasplakinolide at 37°C for 30 min with or without 10 mM methyl-β-cyclodextrin in M1/Glc buffer. Cells were incubated with Mov18 (5μg/ml) for 1 hr on ice followed by secondary antibody labeling for 30 min on ice and imaged directly in M1 buffer. The cells were transfected with Lact C2-GFP or PH-GFP 12-16 hr prior to the experiment. Images were obtained using Olympus FV1000 laser scanning confocal microscope (60X).

Cholesterol and Actin Perturbation

Cholesterol was depleted from cells with saponin (0.1% (w/v) at 4°C for 30 minutes) or mβCD (10 mM at 37°C for 30 minutes), and actin perturbations to generate membrane blebs was carried out using 15μM jasplakinolide (37°C for 30 minutes).

Treatments to Perturb Inner Leaflet Lipids, PIP_2 and PS

To perturb PIP_2, CHO cells were treated with 10 μM Neomycin or Chlorpromazine for 15 min at 37°C prior to the experiment to deplete PIP_2 from the cell surface as described previously (Arbuzova et al., 2000; Raucher and Sheetz, 2001). Briefly, after treatment with the drugs the cells were labeled with PLB for 1 hr on ice and imaged. Live imaging was performed using 100X objective (NA ~1.0) in cells transfected with PH-GFP after addition of 10 μM neomycin at 37°C and images were acquired every minute for 20 min. Alternatively, for PS perturbation, PSA3 cells grown under replete or deplete conditions were treated with 10 μM ionomycin at 37°C for 15 min to activate PS scramblase, and cause PS to flip from inner to outer leaflet (Yeung et al., 2008). The loss of inner leaflet PS was assessed by measuring the extent of PS that is externalized by labeling with Alexa-647 AnnexinV for 1 hr on ice. Images were obtained using 20x (0.75 NA), and quantified using standard routines in Metamorph or analysis was done using a BD FACS Calibur flow cytometer (BD Biosciences) after addition of different PS species.

Mass Spectrometry Experiments

Bleb Isolation

Cells were treated with cytochalasin D (10μg/ml) at 37°C for 20 min in serum free HF-12 media. This was followed by centrifugation at 1,000 g for 5 min; the supernatant obtained was subjected to further centrifugation at 2,000 g for 20 min. The collected pellet (membrane blebs) was used to resuspend in methanol and the lipid extraction was performed.

Lipid Extraction

Cells or blebs isolated from cells were homogenized by adding 500μL of methanol along with internal standards (98pmoles of 17:0/14:1 PI, 85pmoles of 17:0/14:1 PE, 115pmoles of 17:0/14:1 PS and 245 pmoles of 17:0/14:1 PC). The methanolic homogenate was then transferred to an Eppendorf centrifuge tube. This was followed by the addition of 250μL of chloroform and shaken at 1,000 g for 1 hr at 4°C. 250μL of chloroform was further added which was followed by addition of 275μL of ice cold distilled water. The samples were vortexed for 1 min and centrifuged at 10,000 g for 2 min. The organic phase was separated and stored. This was followed by the addition of 500μL chloroform, vortexed for 1 min and centrifuged at 10,000 g for 2 min at 4°C. The organic phase was again isolated and pooled with the earlier fraction. This was then dried and stored at −20°C.

Mass Spectrometric Measurement and Analysis

Mass spectrometric analyses were performed on an LTQ Orbitrap XL instrument (Thermo Fisher Scientific). Stable ESI based ionization of glycerophospholipids was achieved using a robotic nanoflow ion source TriVersa NanoMate (Advion BioSciences) using chips with the diameter of spraying nozzles of 4.1 μm. The ion source was controlled by Chipsoft 8.1.1 software. Ionization voltages were +1.2kV and −1.2kV in positive and negative modes, respectively; back pressure was set at 0.95psi in both modes. The temperature of ion transfer capillary was 180°C. Acquisitions were performed at the mass resolution $R_{m/z400}$ = 100000. Dried total lipid extracts were re-dissolved in 100 μl of chloroform:methanol:water (60:30:4.5). It was further diluted 100 times in MS mix (chloroform:methanol:propanol 1:2:4). For the analysis, 20 μl of samples (n = 6) were loaded onto 96-well plate (Eppendorf) of the TriVersa NanoMate ion source and sealed with aluminum foil. Each sample was analyzed for 10 min in positive ion mode where PC and PE were detected and quantified. This was followed by an independent acquisition in negative ion mode for 10 min where PS and PI were detected and quantified. Data dependent MS/MS measurements were performed as described in Schwudke et al. (2006).

Lipids were identified by LipidXplorer software (Herzog et al., 2011) by matching *m/z* of their monoisotopic peaks to the corresponding elemental composition constraints. Molecular Fragmentation Query Language (MFQL) queries were compiled for all the aforementioned lipid classes. Mass tolerance was 5p.p.m. and intensity threshold was set according to the noise level reported by Xcalibur software (Thermo Scientific).

Atomistic MD Simulations of Multicomponent Asymmetric Bilayer

The procedure and details of our Atomistic MD simulation of a multicomponent bilayer follows the well cited reference of Niemelä et al. (2007) very closely. This has been successfully used in our previous papers (Polley et al., 2012, 2014) to study the physicochemical properties of a multicomponent asymmetric bilayer.

Composition of Model Asymmetric Bilayer

We prepared an asymmetric bilayer membrane comprising POPC, Cholesterol (Chol), PSM in the upper leaflet and POPC, Cholesterol in the lower leaflet at 23°C. The bilayer was embedded in water. We varied the relative concentration (x) of PSM and Chol in the upper leaflet from x (%) = 0 to 25, and the concentration of Chol in the lower leaflet from x (in %) = 0 to 25, the rest being taken up by POPC. This ensures that both the leaflets of the bilayer are always in the ld phase (Polley et al., 2014). We added trace amounts of GPI and PS - 10 GPI molecules in the upper leaflet and 2- 25 molecules of PS in the lower leaflet. We varied the chemistry of GPI and PS by using different lipid chain lengths ($GPI_{C16:0/C16:0}$, $GPI_{C12:0/C12:0}$, $PS_{C18:0/C18:0}$ and $PS_{C12:0/C12:0}$) and nature of saturation ($GPI_{C18:1/C18:1}$ and $PS_{C18:1/C18:1}$). Total number of lipids in the bilayer is 1,024 (512 in each leaflet) surrounded by 32,768 molecules of water (ratio of lipids to water is 1:32), so as to completely hydrate the bilayer.

Initial Configurations

The initial configurations of all the asymmetric multicomponent bilayer membrane were generated using PACKMOL (Martínez et al., 2009). Our MD simulations on the bilayer were carried out from the following initial conditions.

(a) When there is no constraint on GPI or PS, then the initial conditions on the components are (i) all components including GPI and PS are uniformly distributed, (ii) PS is clustered at the center of the lower leaflet while GPI and other components are uniformly distributed, and (iii) GPI and PS are clustered at the center of the upper and lower leaflets, respectively, while the other components are uniformly distributed.

(b) When we cluster and immobilize PS (see below) at the center of the lower leaflet, then the initial conditions on the other components are (i) GPI and other components are uniformly distributed, and (ii) GPI is co-clustered with immobilized PS at the center of the upper leaflet. Immobilization of a molecular species is achieved by setting a high value to its mass without affecting other features of the simulation (see below).

(c) When we cluster and immobilize GPI (see below) at the center of the upper leaflet, then the initial conditions on the other components are (i) PS and other components are uniformly distributed, and (ii) PS is co-clustered with immobilized GPI at the center of the lower leaflet.

Force Fields

The force field parameters for POPC, PSM, PS and Chol have been taken from the previously validated united-atom description (Niemelä et al., 2007; Polley et al., 2012; Tieleman and Berendsen, 1998). The parameters of GPI have been constructed from the previous validated description of glycolipid (Hall et al., 2010). Note that instead of using the full length GPI structure containing five glycan residues (3mannose-Glucosamine-inositol) attached to the glycerolipid, we have used minimal glycan to construct GPI (namely Glucosamine inositol with intact glycerolipid). This is justified by our earlier experiments (unpublished results RR) which showed that modifications of the head group did not affect the nanoclustering of GPI-APs.

PS is a charged lipid with a net charge of −1. To neutralize the entire bilayer membrane system we use Na^+ counter ions.

We use the improved extended simple point charge (SPC/E) model to simulate water molecules, having an extra average polarization correction to the potential energy function.

Long range electrostatic interactions are incorporated by the reaction field method with cut-off r_c = 2nm, while for the Lennard-Jones interactions, we use a cut-off of 1nm.

Choice of Ensembles and Run Times

We use GROMACS (http://www.gromacs.org) (Lindahl et al., 2001) to integrate the Newton's equation of motion with 2fs time step. The asymmetric bilayers are equilibrated for 50ps in the NVT ensemble using a Langevin thermostat to avoid bad contacts arising from steric constraints followed by energy minimization. Then, we run the simulation for 200 ns in the NPT ensemble (T = 296K, p = 1atm). The simulations are carried out in the NPT ensemble for the first 20ns using Berendsen thermostat and barostat, then for 20ns using the Nose-Hoover thermostat and the Parrinello-Rahman barostat to produce the correct ensemble. Subsequent simulations are performed in the NPT ensemble using Berendsen thermostat. We use a semi-isotropic pressure coupling with compressibility 4.5×10^{-5} bar^{-1} for the simulations in the NPT ensemble.

Pairwise forces were calculated by rerunning the trajectory with a cut-off of 2nm for electrostatic interactions. We employed the LINCS algorithm to constrain the bond lengths (Hess et al., 1997) and the SETTLE algorithm to keep the water molecules rigid (Miyamoto and Kollman, 1992) so that an integrator time step of 2fs could be used.

For each initial configuration, we run the simulations for 200 ns before computing the desired physical quantities, over the last 50ns of the trajectories. We have reconfirmed the results of the 200 ns simulations by running key representative cases for 1 μs, looking at mechanical and thermodynamic stability, approach to equilibrium, instability of initial clustered configurations and compositional segregation and approach to homogenization.

Protocol for Immobilization

In the absence of gravity, the mass of the constituents does not enter into equilibrium statistical mechanics. It will however enter in the dynamics or approach to unconstrained equilibrium. Therefore, we increase the mass of either GPI or PS – this will make the dynamics of this molecular species very slow, effectively immobilizing the molecule over the timescale of simulation. The other molecular species are free to move in the presence of these immobilized species. The late time configuration could be thought of as a constrained equilibrium configuration.

To create an immobilized lipid, we use the following protocol. We first determine that the P-atom of the head group of GPI/PS lipid is closest to center-of-mass of the lipid. We then increase the mass of this P-atom of the particular lipid by a factor of 1,000, keeping everything else (parameters of bonded and non-bonded interactions etc.) the same in the parameter file. While this effectively immobilizes the center-of-mass of the lipid, it leaves it free to explore variations in chain configuration and orientation. The initial configuration of these immobilized species is taken from a previously generated typical equilibrium run.

Equilibration and Stability of Bilayer Membrane

We ensure as far as we can, that the model membrane is mechanically stable, tensionless and thermally equilibrated, with no flip-flop over the time scales of the simulation. We have computed the time series of the force and torque components, surface tension, area per lipid, and energy density over 200 ns, and have determined that we are at or close to thermodynamic equilibrium. Since the membrane is macroscopically maintained in the *ld* phase, the equilibration time from the uniform initial configuration is very fast.

We have measured the stress profiles using Irving-Kirkwood contour dividing the bilayer in 0.1nm thick slabs. The pressure profiles are generated from trajectories over 50ns using SHAKE algorithm (Ryckaert et al., 1977) to constrain bond lengths.

To ensure mechanical equilibrium, we compute the components of the net force and torque of the bilayer membrane. This is computed from the local stress tensor $\sigma_{ij}(x,y,z)$ defined through the virial using the standard procedure [see for e.g., (Polley et al., 2012, 2014)] The coarse-grained volume used in the computation of local stress is $v = [0.1nm]^3$.

The components of the net force F_i and net torque M_{ij} where i, j, k runs from 1, 2, 3 (corresponding to the x, y and z components; x,y being the plane of the membrane) can now be simply calculated as derivatives of the stress tensor and its first moment and integrating over the bilayer. Force and torque balance ensures mechanical equilibrium.

The surface tension of the bilayer can be computed from the lateral pressure integrated over the width of the bilayer (Polley et al., 2014). The lateral pressure in turn is computed from the appropriate combination of the components of the stress tensor. We have to ensure that the membrane in the unconstrained system is tensionless. On the other hand, the constraint that PS is immobile and clustered at the center should induce a tension in the membrane.

Below we tabulate the values of the components of net force, torque and surface tension for a typical asymmetric bilayer composition at three different conditions.

Tabulation of Force, Torque, and Surface Tension for the Multicomponent Bilayer Membrane

The composition of the asymmetric bilayer is chosen to be, Upper leaflet 15% PSM (Chol) and rest POPC with 10 long chain GPI; and Lower leaflet: 15% of Chol and rest POPC with 15 long chain PS. The force, torque and surface tension are evaluated at 200 ns.

Condition 1: GPI and PS unconstrained. Initial condition is where all components are uniformly distributed.

F_1 (nN)	F_2 (nN)	F_3 (nN)	M_{12} (nN.nm)	M_{13} (nN.nm)	M_{23} (nN.nm)	Υ (bar.nm)
1.141 ± 1.017	1.101 ± 1.108	0.851 ± 0.650	0.911 ± 0.081	0.495 ± 0.019	0.119 ± 0.052	−0.021 ± 0.016

Condition 2: PS clustered and immobilized at the center of the lower leaflet. All other components including GPI are initially uniformly distributed on the bilayer.

F_1 (nN)	F_2 (nN)	F_3 (nN)	M_{12} (nN.nm)	M_{13} (nN.nm)	M_{23} (nN.nm)	Υ (bar.nm)
−1.45 ± 0.109	0.34 ± 0.115	−0.18 ± 0.076	0.791 ± 0.015	−0.98 ± 0.021	−0.97 ± 00.013	−0.13 ± 0.018

Condition 3: PS clustered and immobilized at the center of the lower leaflet. GPI is clustered above PS on the bilayer.

F_1 (nN)	F_2 (nN)	F_3 (nN)	M_{12} (nN.nm)	M_{13} (nN.nm)	M_{23} (nN.nm)	Υ (bar.nm)
−0.25 ± 0.019	0.79 ± 0.111	0.92 ± 0.121	0.47 ± 0.017	0.99 ± 0.014	0.69 ± 0.009	−0.23 ± 0.012

The tabulated values of force and torque components shown above are comparable to the values computed for the mechanically stable single component (POPC) symmetric bilayer (Polley et al., 2012, 2014), where we found that $F_1 = 0.83 \pm 1.66$nN, $F_2 = 0.27 \pm 1.14$nN, $F_3 = -0.16 \pm 1.25$nN and $M_{12} = 8.26 \pm 0.102$nN.nm, $M_{13} = 10.74 \pm 0.066$nN.nm, $M_{23} = 9.33 \pm 0.094$nN.nm. On the other hand, while the symmetric bilayer at equilibrium was tensionless, with the computed $\Upsilon = 0.0204 \pm 0.0357$bar.nm, the surface tensions computed in the case where PS is constrained is larger than this.

Area per Lipid, A_h

We collect the positions of all lipids in each leaflet and project on the x-y plane (plane of the membrane) from which we find the box size and total area occupied by all lipids in each leaflet. By dividing these two, we get the mean area per lipid of the bilayer.

Total Energy, E

We use GROMACS in-built analysis (g_energy) tools; we calculate total energy which is the sum over all the particle's potential energy and kinetic energy of the system with time to monitor the equilibration of the system.

Computation of Deuterium Order Parameter, S

We calculate the spatial distribution of the deuterium order parameter, S from the selected carbon atoms (C5-C7) of each acyl chain (including *sn1* and *sn2* chains) of the GPI, PS, PSM and POPC lipids (Polley et al., 2012, 2014). This is then coarse-grained (binned) over a spatial scale of 1nm for the last 50 ns of the trajectory of the simulations. The circular averaged deuterium order parameter profile in the upper and lower leaflets, S_u and S_l, are then plotted against the radial dimension r which goes from 0 (at the center) to the edge (L) of the membrane.

Computation of Number Density, ρ

We calculate the spatial number density, ρ from the coordinate of the center of mass of the lipids in each leaflet from the final 50 ns of the trajectory. We project the positions of the center of mass of the lipids on x-y plane and bin it with a grid size of 1nm to calculate spatial number density. The circular averaged density profile is then plotted against the radial dimension r which goes from 0 (at the center) to the edge (L) of the membrane.

Computation of Transbilayer Correlation Coefficient, C_{ul}

The transbilayer correlation coefficient, C_{ul} is computed from the normalized transbilayer correlation (Polley et al., 2014) (r denotes the 2d coordinate (x,y)),

$$C_{ul}(\rho_u(x,y)\rho_l(x,y)) = \frac{\langle \rho_u(x,y)\rho_l(x,y)\rangle - \langle \rho_u(x,y)\rangle\langle \rho_l(x,y)\rangle}{\sqrt{\left\langle \rho_u(x,y)^2\right\rangle - \langle \rho_u(x,y)\rangle^2}\sqrt{\left\langle \rho_l(x,y)^2 - \rho_l(x,y)\right\rangle^2}}$$

averaged over space, where $\rho_u(x,y)$ and $\rho_l(x,y)$ are the local density of the GPI and PS at upper and lower leaflet, respectively. The same grid size, namely 1nm, is used to calculate C_{ul}.

Computation of Coherence Length

The coherence length (ξ) of the density and order parameter is extracted from the exponential fall off of this quantity from the center of the leaflet (marked 0), in the condition where PS is clustered and immobilized at the center and GPI are initially co-clustered at the center (Polley et al., 2012, 2014).

SUPPLEMENTAL REFERENCES

Bandyopadhyay, S., and Bong, D. (2011). Synthesis of trifunctional phosphatidylserine probes for identification of lipid-binding proteins. Eur. J. Org. Chem., 751–758.

Hall, A., Róg, T., Karttunen, M., and Vattulainen, I. (2010). Role of glycolipids in lipid rafts: a view through atomistic molecular dynamics simulations with galactosylceramide. J. Phys. Chem. B *114*, 7797–7807.

Herzog, R., Schwudke, D., Schuhmann, K., Sampaio, J.L., Bornstein, S.R., Schroeder, M., and Shevchenko, A. (2011). A novel informatics concept for high-throughput shotgun lipidomics based on the molecular fragmentation query language. Genome Biol. *12*, R8.

Hess, B., Bekker, H., Berendsen, H.J.C., and Fraaije, J.G.E.M. (1997). LINCS: A linear constraint solver for molecular simulations. J. Comput. Chem. *18*, 1463–1472.

Johnson, C.L., and Guo, Z. (2013). Synthesis of novel, fluorescently tagged analogs of glycosylphosphatidylinositol (GPI). Anchors. J. Carbohydr. Chem. *32*, 301–323.

Lindahl, E., Hess, B., and van der Spoel, D. (2001). GROMACS 3.0: a package for molecular simulation and trajectory analysis. J. Mol. Model *7*, 306–317.

Martínez, L., Andrade, R., Birgin, E.G., and Martínez, J.M. (2009). PACKMOL: a package for building initial configurations for molecular dynamics simulations. J. Comput. Chem. *30*, 2157–2164.

Miyamoto, S., and Kollman, P.A. (1992). SETTLE: an analytical version of the SHAKE and RATTLE algorithm for rigid water models. J. Comput. Chem. *13*, 952–962.

Niemelä, P.S., Ollila, S., Hyvönen, M.T., Karttunen, M., and Vattulainen, I. (2007). Assessing the nature of lipid raft membranes. PLoS Comput. Biol. *3*, e34.

Ryckaert, J.-P., Ciccotti, G., and Berendsen, H.J. (1977). Numerical integration of the cartesian equations of motion of a system with constraints: molecular dynamics of *n*-alkanes. J. Comput. Phys. *23*, 327–341.

Saikam, V., Raghupathy, R., Yadav, M., Gannedi, V., Singh, P.P., Qazi, N.A., Sawant, S.D., and Vishwakarma, R.A. (2011). Synthesis of new fluorescently labeled glycosylphosphatidylinositol (GPI) anchors. Tetrahedron Lett. *52*, 4277–4279.

Schwudke, D., Oegema, J., Burton, L., Entchev, E., Hannich, J.T., Ejsing, C.S., Kurzchalia, T., and Shevchenko, A. (2006). Lipid profiling by multiple precursor and neutral loss scanning driven by the data-dependent acquisition. Anal. Chem. *78*, 585–595.

Sengupta, P., Balaji, J., and Maiti, S. (2002). Measuring diffusion in cell membranes by fluorescence correlation spectroscopy. Methods *27*, 374–387.

Tieleman, D.P., and Berendsen, H.J. (1998). A molecular dynamics study of the pores formed by *Escherichia coli* OmpF porin in a fully hydrated palmitoyloleoylphosphatidylcholine bilayer. Biophys. J. *74*, 2786–2801.

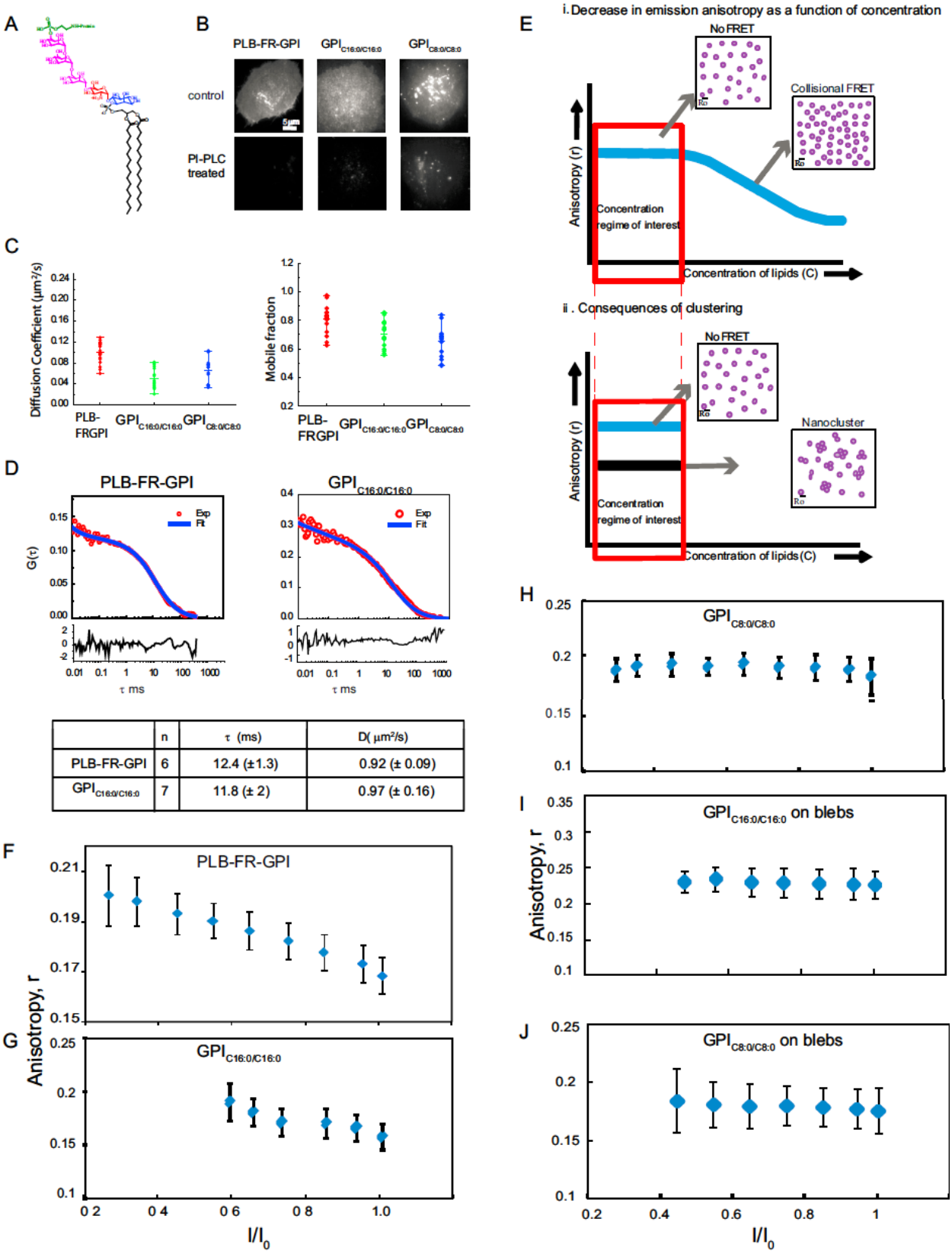

	n	τ (ms)	D(μm²/s)
PLB-FR-GPI	6	12.4 (±1.3)	0.92 (± 0.09)
$GPI_{C16:0/C16:0}$	7	11.8 (± 2)	0.97 (± 0.16)

Figure S1. Characterization of Exogenously Incorporated GPI Analogs, Related to Figure 1

(A) Schematic represents the chemical structure of full length GPI (ethanolamine coupled via a phosphodiester linkage to the terminal mannose of a trimannose oligosaccharide, in turn linked to glucosamine-PI).

(B) Micrographs show fluorescence intensity images of FR-GPI expressing CHO cells (IA2.2F) labeled with either PLB bound to FR-GPI or with exogenously incorporated Bodipy^{TMR} tagged GPI analogs, as indicated, pre (control) or post PI-PLC treatment. The loss of all detectable fluorescence shows that the GPI-analogs are mainly distributed at the outer leaflet of the cells, similar to endogenous GPI-anchored proteins.

(C) Diffusion coefficients (left panel) and mobile fraction (right panel) of PLB-labeled FR-GPI or indicated GPI analogs in IA2.2F cells, obtained from FRAP measurements show that the exogenously incorporated lipids behave very similar to the endogenous GPI-anchored proteins.

(D) Autocorrelation curves and fits obtained from MEM analysis for both PLB-FR-GPI and $GPI_{C16:0/C16:0}$ are plotted. The table indicates the diffusion time scales [τ(D)] and diffusion coefficient (D) obtained from the MEM analysis. n = number of independent measurements, values in parenthesis denotes standard deviation.

(E) Idealized profiles of the expected change in fluorescence emission anisotropy of labeled lipids with a systematic increase in concentration, as determined previously (Sharma et al., 2004). Note at very low concentration, the fluorescent lipid molecules are far apart and do not undergo FRET, and hence maintain a regime of constant anisotropy. As the concentration increases beyond a critical range, the fluorescent lipids can undergo homo-FRET due to the enhanced density of neighboring molecules, and the emission anisotropy decreases. However if the fluorescent lipid species are pre-clustered at a distance where they can engage in homo-FRET, the emission anisotropy exhibits a low value even in the concentration regime where concentration dependent depolarization is not expected. The concentration range marked with a red box is the regime at which anisotropy of GPI lipids are measured in all experiments.

(F–J) FR-GPI expressing CHO cells were labeled with PLB (F), or incorporated with exogenously added $GPI_{C16:0/C16:0}$ (G, I) or $GPI_{C8:0/C8:0}$ (H, J), photobleached and the fluorescence emission anisotropy recorded during the bleaching process. Membrane blebs (I, J) were created on $GPI_{C16:0/C16:0}$ or $GPI_{C8:0/C8:0}$ incorporated cells and bleached in a similar fashion. Note the profiles of change in emission anisotropy upon change in fluorescence intensity; PLB-FR-GPI and $GPI_{C16:0/C16:0}$ exhibit a similar linear increase (F, G), characteristic of nanoclustered fluorophores (Sharma et al., 2004), while $GPI_{C8:0/C8:0}$ on cell membranes (H) or membrane blebs (J) and $GPI_{C16:0/C16:0}$ on membrane blebs (I) exhibit no change, indicating the lack of homo-FRET. The starting intensity for all the examples collected here are similar and normalized to that used in the first frame. The error bars represent SD.

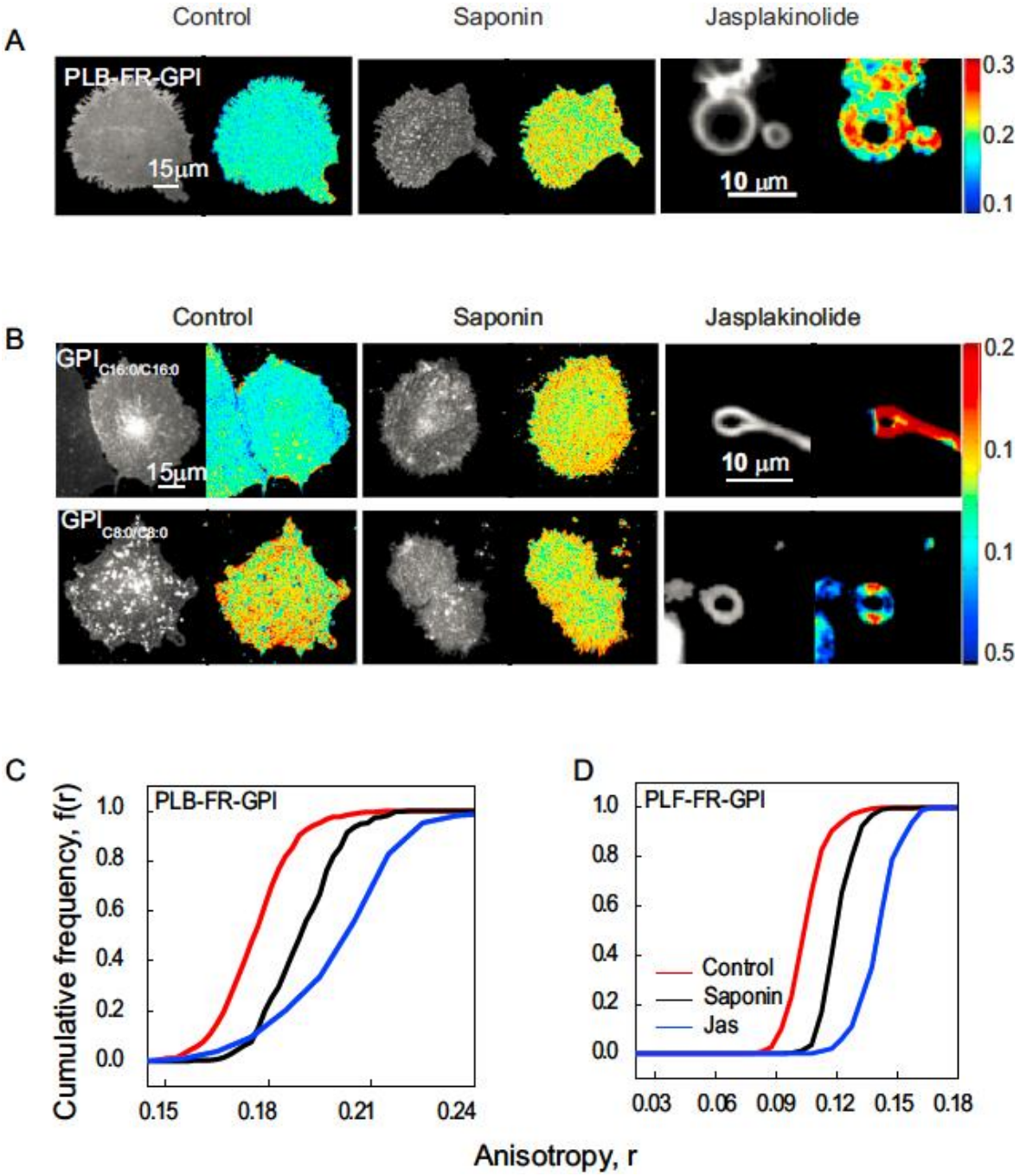

Figure S2. Cholesterol Depletion and Actin Perturbation of Fluorescently Tagged Folates and GPI Analogs, Related to Figure 1

(A and B) Fluorescence intensity and anisotropy images of IA2.2F cells labeled with PLB (GPI-AP) or with exogenously incorporated Bodipy^{TMR} conjugated GPI analogs ($GPI_{C16:0/C16:0}$ or $GPI_{C8:0/C8:0}$; see structures in Figure 1A) post-cholesterol depletion (saponin) or generation of membrane blebs (jas) or without any treatment (control) show the systematic change in anisotropy due to these perturbations.

(C and D) Cumulative frequency distribution (CFD) plots of fluorescence emission anisotropy of FR-GPI-expressing CHO (IA2.2F) cells labeled with PLB (C) and PLF (D) from untreated (control, red line) cells, cells treated with saponin (black line), or from membrane blebs derived via jasplakinolide treatment (blue line) demonstrate the effects of cholesterol depletion and actin perturbation on GPI-anchored protein clustering. Fluorescence intensity and anisotropy, as well as CFD plots from data derived from images such as these, are shown in Figures 1B and 1D. Note that, unlike the GPI-AP and $GPI_{C16:0/C16:0}$ analog, the $GPI_{C8:0/C8:0}$ analog exhibits no change in its emission anisotropy as also observed in the CFD plots in Figure 1 (D).

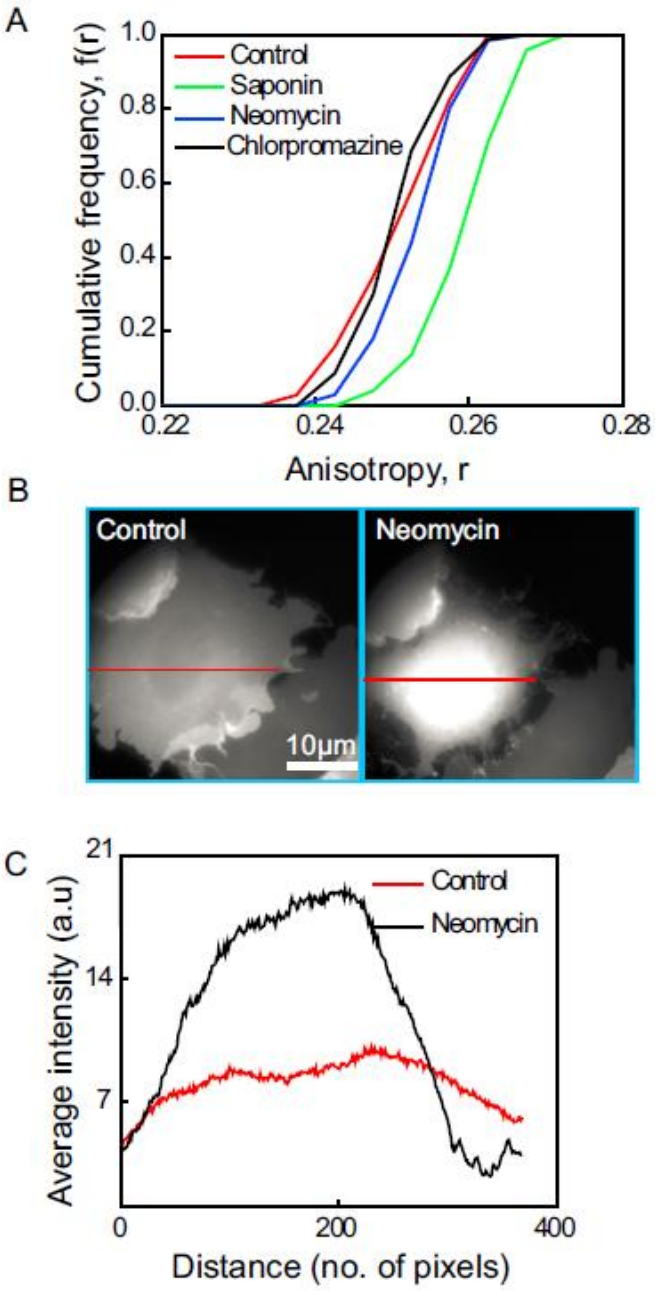

Figure S3. GPI-Anchored Protein Nanoclustering Is Insensitive to PI(4,5)P_2 Levels at the Plasma Membrane, Related to Figure 3

(A) CFD plots for PLB-FR-GPI in IA2.2F cells in untreated (red line), neomycin (blue), or chlorpromazine (black line)- and saponin-treated (green line) cells show that treatments that reduce PI(4,5)P_2 at the cell surface have no effect on the emission anisotropy of GPI-APs.

(B and C) Images (B) and line intensity profile (C) of PH-GFP transfected in IA2.2F cells under control (red line in (C) and neomycin (black line in [C] treated conditions) indicate that neomycin treatment dramatically redistributes PLCδ-PH-GFP, a PI(4,5)P_2 binding domain, from the plasma membrane to the cytoplasm. Red line in (B) depicts the region of line scan measurements.

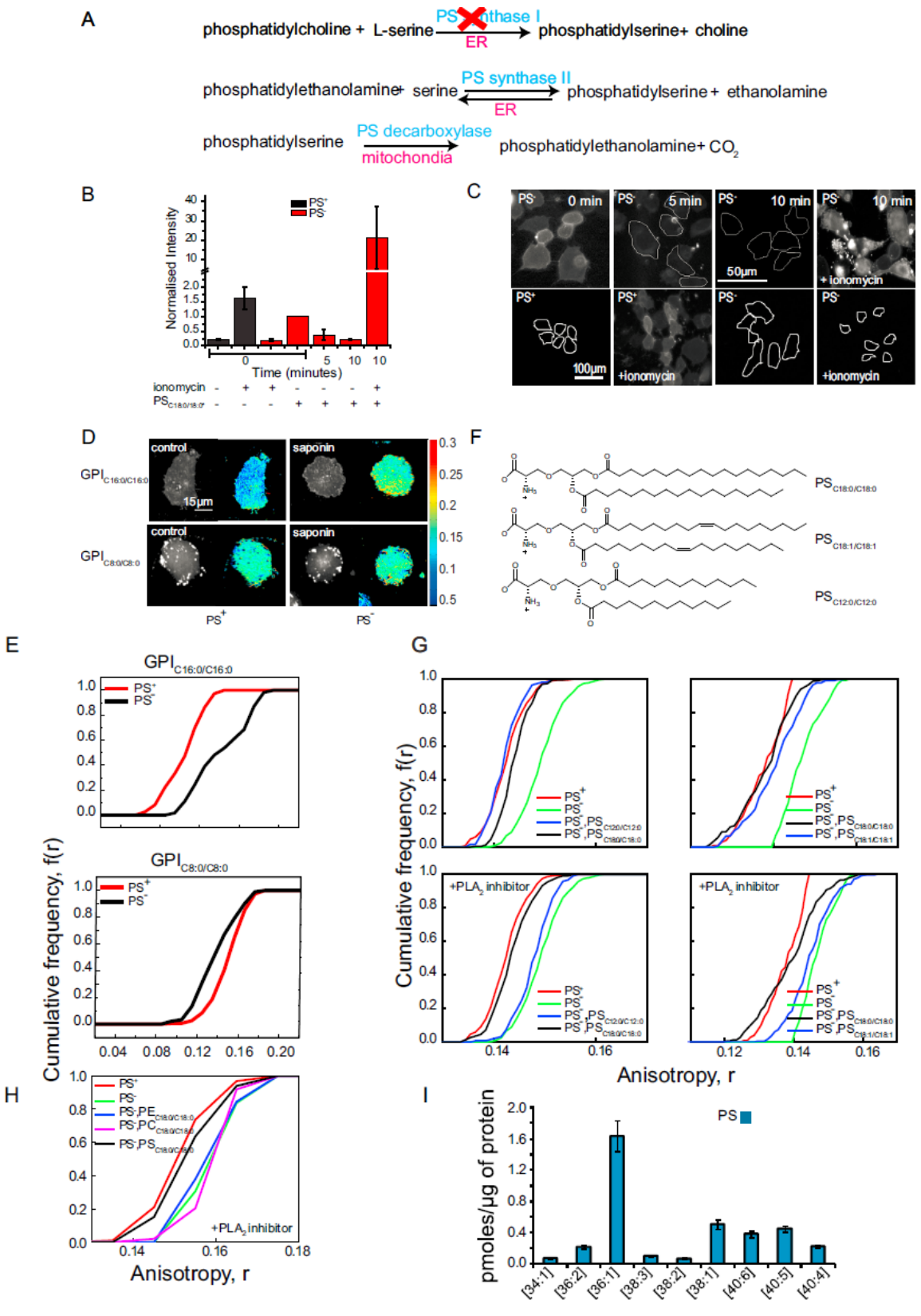
A
phosphatidylcholine + L-serine
PS synthase I
ER
phosphatidylserine + choline
phosphatidylethanolamine + serine
PS synthase II
ER
phosphatidylserine + ethanolamine
phosphatidylserine
PS decarboxylase
mitochondia
phosphatidylethanolamine + CO2
B
Normalised Intensity
Time (minutes)
ionomycin
PS C18:0/18:0
C
0 min
5 min
10 min
10 min
50µm
+ ionomycin
100µm
+ionomycin
D
control
saponin
15µm
GPI C16:0/C16:0
GPI C8:0/C8:0
F
PS C18:0/C18:0
PS C18:1/C18:1
PS C12:0/C12:0
E
GPI C16:0/C16:0
GPI C8:0/C8:0
Cumulative frequency, f(r)
G
+PLA2 inhibitor
Anisotropy, r
H
PS+
PS-
PS-;PE C18:0/C18:0
PS-;PC C18:0/C18:0
PS-;PS C18:0/C18:0
+PLA2 inhibitor
Anisotropy, r
I
pmoles/µg of protein
PS
[34:1]
[36:2]
[36:1]
[38:3]
[38:2]
[38:1]
[40:6]
[40:5]
[40:4]

Figure S4. PS Analogs Restore GPI-Anchored Protein Nanoclustering in PSA3 Cells, Related to Figure 4

(A) Schematic shows the biosynthetic pathway of PS in mammalian cells and the step at which the mutation in PSS1 enzyme disrupts PS synthesis in PSA3 cells.
(B and C) Histogram (B) shows quantification of fluorescence intensity images (C) of AnnexinV staining in PSA3 cells incubated at 37°C without or with ionomycin and/or incorporated with $PS_{C18:0/C18:0}$* in PS replete and deplete conditions, as indicated. The fluorescence intensity values obtained were normalized to that obtained from cells incorporated with the lipid prior to incubation at 37°C (0 min). Data are obtained from 200 cells from 2 experiments. Note that, after 10 min at 37°C, most of the exogenously incorporated PS is present in the lower leaflet of the cells and is detected by Annexin V labeling only upon externalization by activation of scramblase with ionomycin.
(D and E) Fluorescence intensity images (D) and CFD plot (E) for fluorescent GPI-analogs $GPI_{C16:0/C16:0}$ or $GPI_{C8:0/C8:0}$ incorporated in PSA3 cells in the replete (PS^+) (red line) or deplete (PS^-) (black line) conditions. Note that $GPI_{C16:0/C16:0}$ lipid exhibits a PS-dependent emission anisotropy, whereas the emission anisotropy of $GPI_{C8:0/C8:0}$ is unchanged in PS replete (PS^+) and deplete (PS^-) conditions.
(F–H) (F) Chemical structure of PLA_2-sensitive PS analogs used in this study (G) CFDs of emission anisotropy of A488F-labeled PSA3 cells grown under PS repleted (PS^+) (red line) or PS depleted (PS^-) (green line) conditions, when PS of varying chain lengths (blue or black line) or (H) when PC (magenta line) or PE (blue line) were incorporated into the cell in the absence or presence of PLA_2 inhibitor as indicated. Note that GPI-anchored protein emission depolarization is restored in all cases with the addition of PS variants, whereas in the presence of PLA_2-inhibitor only the long saturated acyl chain containing PS analog support emission depolarization, consistent with nanoclustering. Incorporation of equal amount of PC or PE did not restore GPI-AP nanoclustering in these cell lines.
(I) Histogram shows the amount of different PS species which are present in PSA3 cells grown under PS repleted (PS^+) conditions.
The error bars represent SEM.

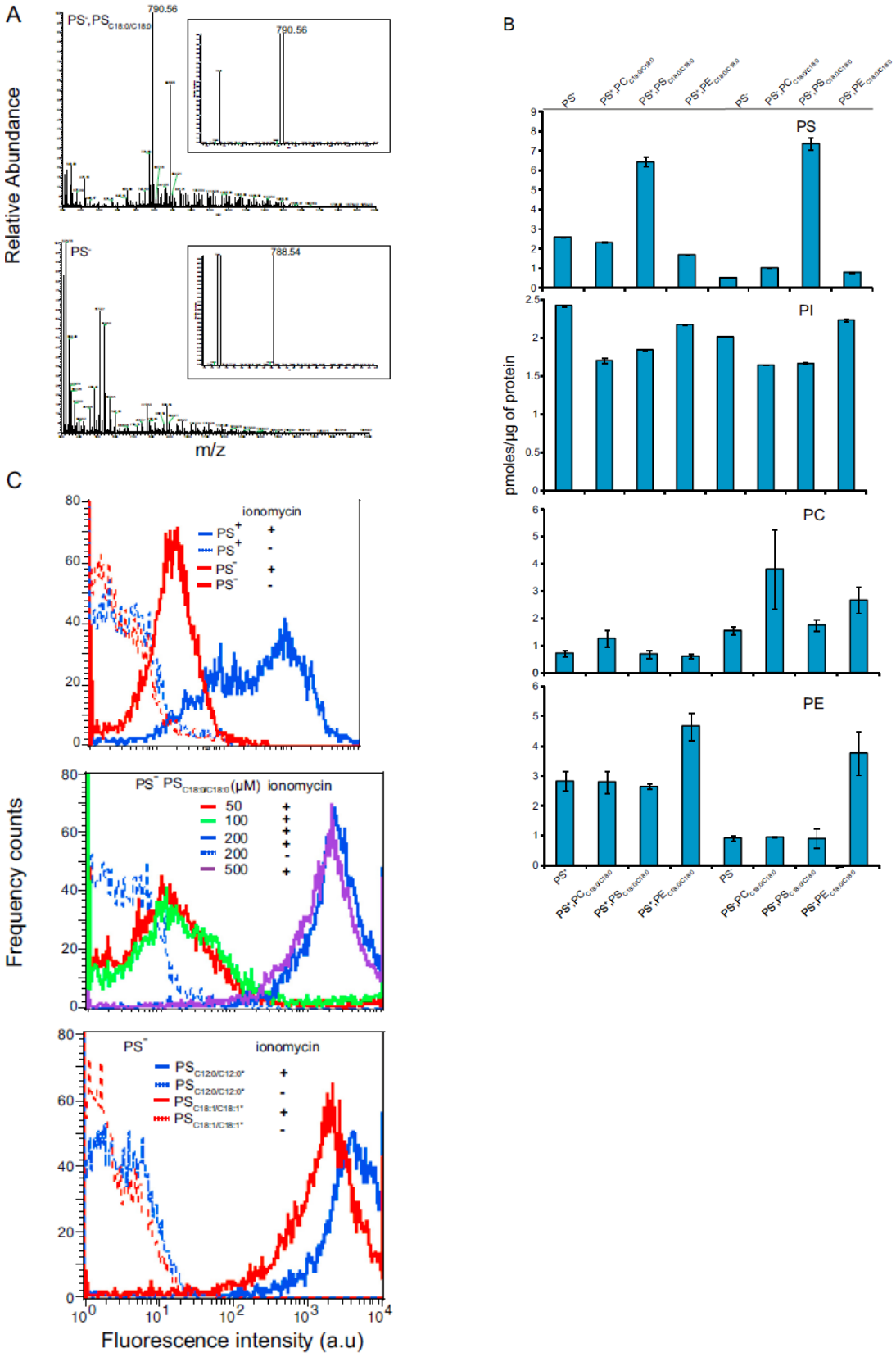
A
Relative Abundance
PS-; PS C18:0/C18:0
790.56
790.56
PS-
788.54
m/z
B
PS-
PS-; PC C18:0/C18:0
PS-; PS C18:0/C18:0
PS-; PE C18:0/C18:0
PS-
PS-; PC C18:0/C18:0
PS-; PS C18:0/C18:0
PS-; PE C18:0/C18:0
PS
PI
PC
PE
pmoles/µg of protein
C
ionomycin
PS+ +
PS+ -
PS- +
PS- -
PS- PS C18:0/C18:0 (µM) ionomycin
50 +
100 +
200 +
200 -
500 +
PS-
ionomycin
PS C12:0/C12:0* +
PS C12:0/C12:0* -
PS C18:1/C18:1* +
PS C18:1/C18:1* -
Frequency counts
Fluorescence intensity (a.u)

Figure S5. Mass Spectrometric and FACS Measurements Showing the Level of Incorporation of Different Species of PS, PE, and PC, Related to Figure 4

(A and B) Representative mass spectra showing with (A) or without (B) the incorporation of $PS_{C18:0/C18:0}$ (m/z: 790.56) in PS deplete (PS^{-}) cells. The inset shows the close up of the $PS_{C18:0/C18:0}$ peak at m/z of 790.56. Note that this peak is absent in (B). Histogram (B) showing the amount of exogenously incorporated lipid species (PS, PI, PC and PE as indicated) present in membrane blebs generated from cells after incorporation of various species of lipids as indicated. Lipids were incorporated as described in Saha et al. (2015) (Figure 4).

(C) FACs profiles of Alexa647-Annexin V binding to cells were obtained from cells incorporated with different species of PS, or concentration of PS obtained either before or after-ionomycin treatment as indicated.

The error bars represent SEM.

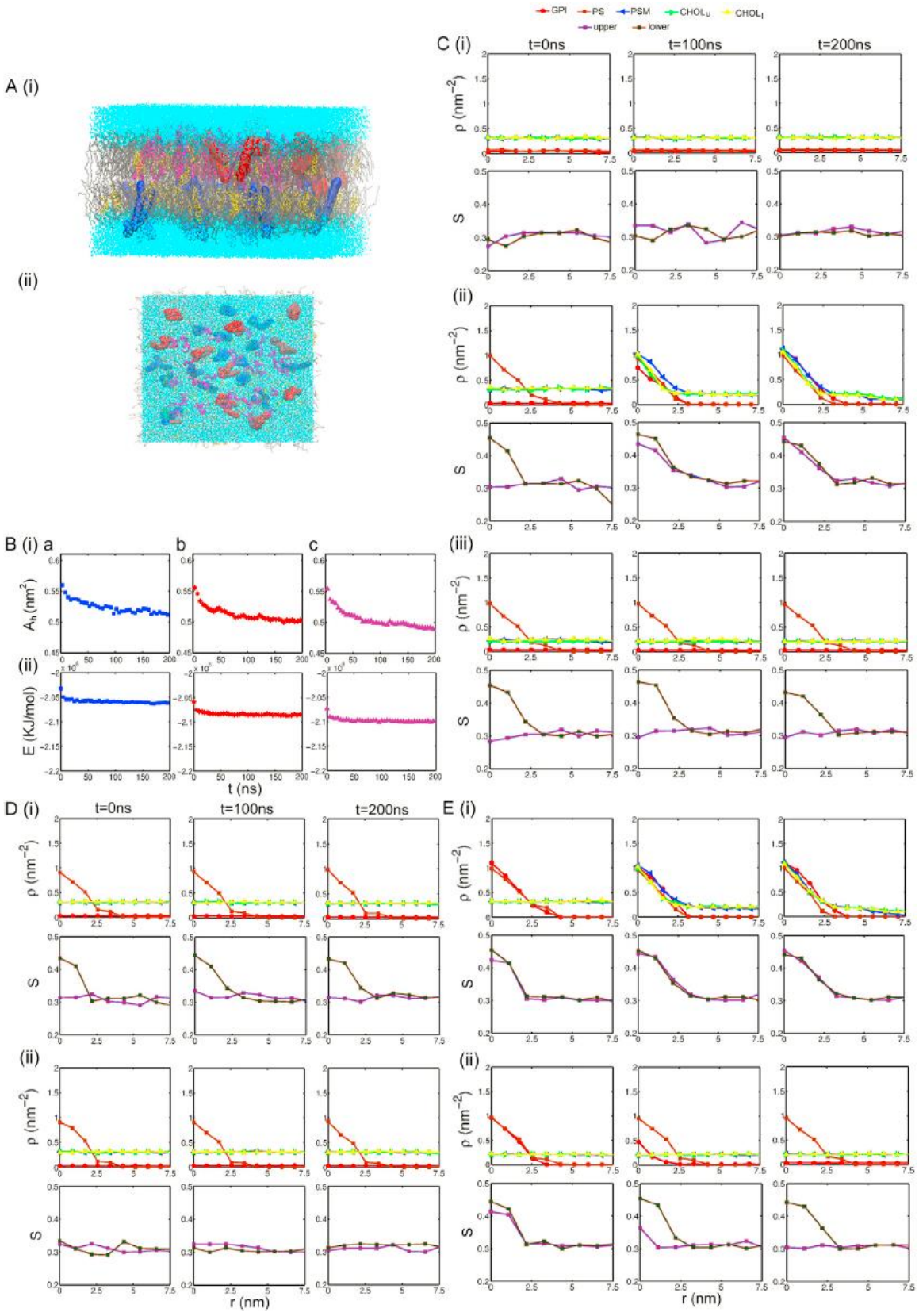
A (i)
(ii)
B (i) a
b
c
(ii)
A_h (nm^2)
E (KJ/mol)
t (ns)
C (i)
t=0ns
t=100ns
t=200ns
GPI
PS
PSM
CHOL$_u$
CHOL$_l$
upper
lower
ρ (nm^{-2})
S
(ii)
(iii)
D (i)
(ii)
r (nm)
E (i)
(ii)
r (nm)

Figure S6. All-Atom MD Simulations of an Asymmetric, Multicomponent Bilayer, Related to Figure 5

(A) Late time configurations of an asymmetric bilayer composed of POPC (gray), PSM (magenta), Chol (yellow), GPI (red), and PS (blue) embedded in water (cyan) from MD simulations in the *ld*-phase, when neither GPI nor PS is constrained. (i) Upper leaflet comprises 4% PSM, 4% Chol, 10 long saturated $GPI_{C16:0/C16:0}$ and the rest POPC, while lower leaflet has 35% Chol, 25 long saturated $PS_{C18:0/C18:0}$ and rest POPC. (ii) Enface view of the bilayer (bottom) shows uniform distribution of PS and GPI, consistent with being in the *ld*-phase.

(B) The approach to equilibrium is monitored by the time evolution of (i) the mean area per lipid (A_h) and (ii) the mean energy (E) over 200 ns in typical simulation runs and reconfirmed in longer 1 μs runs. The asymmetric bilayer composition is fixed at (*upper leaflet*) 15% PSM, 15% Chol, rest POPC with 10 GPI and (*lower leaflet*) 15% Chol, rest POPC with 15 PS. The panels (a)-(c) indicate different ensembles and initial conditions: (a) GPI and PS are unconstrained with initial condition such that all components, including GPI and PS are distributed uniformly. (b) PS is immobilized at the center of the lower leaflet with initial condition where all other components including GPI are distributed uniformly, (c) PS is immobilized at the center of the lower leaflet with initial condition where GPI is co-clustered with PS at the upper leaflet.

(C) Dynamics toward co-clustering of GPI and PS monitored by the profiles of all membrane compositions (ρ) and deuterium order parameter (S) of the upper (S_u) and lower (S_l) leaflets at the indicated time points 0 ns (left panels), 100 ns (middle panels) and 200 ns (right panel) under different conditions: (i) Starting from a configuration where all the components including GPI and PS are uniformly distributed across the entire membrane from the center to the edge, [0,|L/2|] and a bilayer with 15% PSM (cholesterol) and rest POPC with 10 GPI at the upper leaflet, and 15% cholesterol and rest POPC with 15 PS at the lower leaflet, the spatial profile attained by t = 200 ns (and reconfirmed in the longer 1 μs runs), is uniform and homogeneous with no sign of co-segregation of GPI and PS, consistent with the membrane being in the *ld* phase. (ii) Same composition and initial configuration as (i), except for PS which is held immobile at the center (0 on the x axis) of the lower leaflet. The profiles attained at 200 ns show that GPI, cholesterol and PSM co-segregate with the immobilized PS to attain bilayer registry. Simultaneously, the deuterium order parameters in the two leaflets S_u and S_l, show a high value in this region. Note the membrane and cholesterol composition in the two leaflets are in the gray region of Figure 5C. (iii) The bilayer is now 10% PSM, 10% Chol and rest POPC with 10 GPI at the upper leaflet, and 10% cholesterol and rest POPC with 15 PS at the lower leaflet located in the green region of Figure 5C. The initial configuration is same as (ii), the spatial profiles attained at 200 ns show that the upper leaflet constituents are uniformly distributed with no sign of bilayer registry. This is also apparent in the profile of the deuterium order parameter S_u. These observations highlight the role of immobilization and membrane composition in permitting co-segregation and bilayer registry of constituents in the upper and lower leaflets of a bilayer in an *ld* phase. Colored symbols indicated in legend at the top denote the indicated components.

(D) Stability of co-segregated configuration as a function of cholesterol levels, monitored by profiles of all membrane compositions (ρ) and deuterium order parameter (S). (i) The bilayer has 15% PSM, 15% Chol and rest POPC with 10 GPI at the upper leaflet, and 15% cholesterol and rest POPC with 15 PS at the lower leaflet. Cholesterol composition in the two leaflets is in the gray region of Figure 5C. Initial configuration such that both upper leaflet GPI and lower leaflet PS are clustered at the center, but only PS is held immobile throughout the simulation. The spatial profiles at 200 ns show that GPI, cholesterol and PSM remain co-segregated with the immobilized PS and maintains bilayer registry. This is reflected in the profile of the deuterium order parameter in the upper leaflet S_u. The density profile at 200 ns obtained under these conditions are used to determine the coherence lengths (Figure 5D). These results is reconfirmed by our longer 1 μs runs. (ii) The bilayer has 10% PSM, 10% Chol and rest POPC with 10 GPI at the upper leaflet, and 10% Chol and rest POPC with 15 PS at the lower leaflet. Cholesterol composition in the two leaflets is in the gray region of Figure 5C. Initial conditions and immobilization of PS same as above. The spatial profiles at 200 ns show that GPI, Cholesterol and PSM fail to maintain co-segregation with the immobilized PS and evolve toward a uniform distribution on the membrane. Both our 200 ns and longer 1 μs runs indicate that the initial clustering of GPI and PSM is unstable. This is also reflected in the profile of the deuterium order parameter in the upper leaflet S_u.

(E) Dependence of dynamics of co-segregation of GPI and PS on changes in lipid chemistry monitored by profiles of all membrane compositions (ρ) and deuterium order parameter (S). The bilayer has an upper leaflet composition of 15% PSM, 15% Chol and rest POPC with either 10 GPI molecules with (i) short acyl chains or (ii) long acyl chains, or a lower leaflet composition of 15% cholesterol and rest POPC with 15 PS with (i) long acyl chains or (ii) short acyl chains. The initial configuration is such that all components with the exception of PS are uniformly distributed, while PS is held immobile at the center of the lower leaflet (0 on the x axis) at all times. The spatial profiles at 200 ns show that short chain GPI in the upper leaflet do not co-segregate with PS in (i), nor do the short chain PS at the lower leaflet co-segregate with GPIs in the upper leaflet in (ii). This is also reflected in the profile of the deuterium order parameter in the upper leaflet S_u. Colored symbols indicated in legend at the top denote the indicated components.

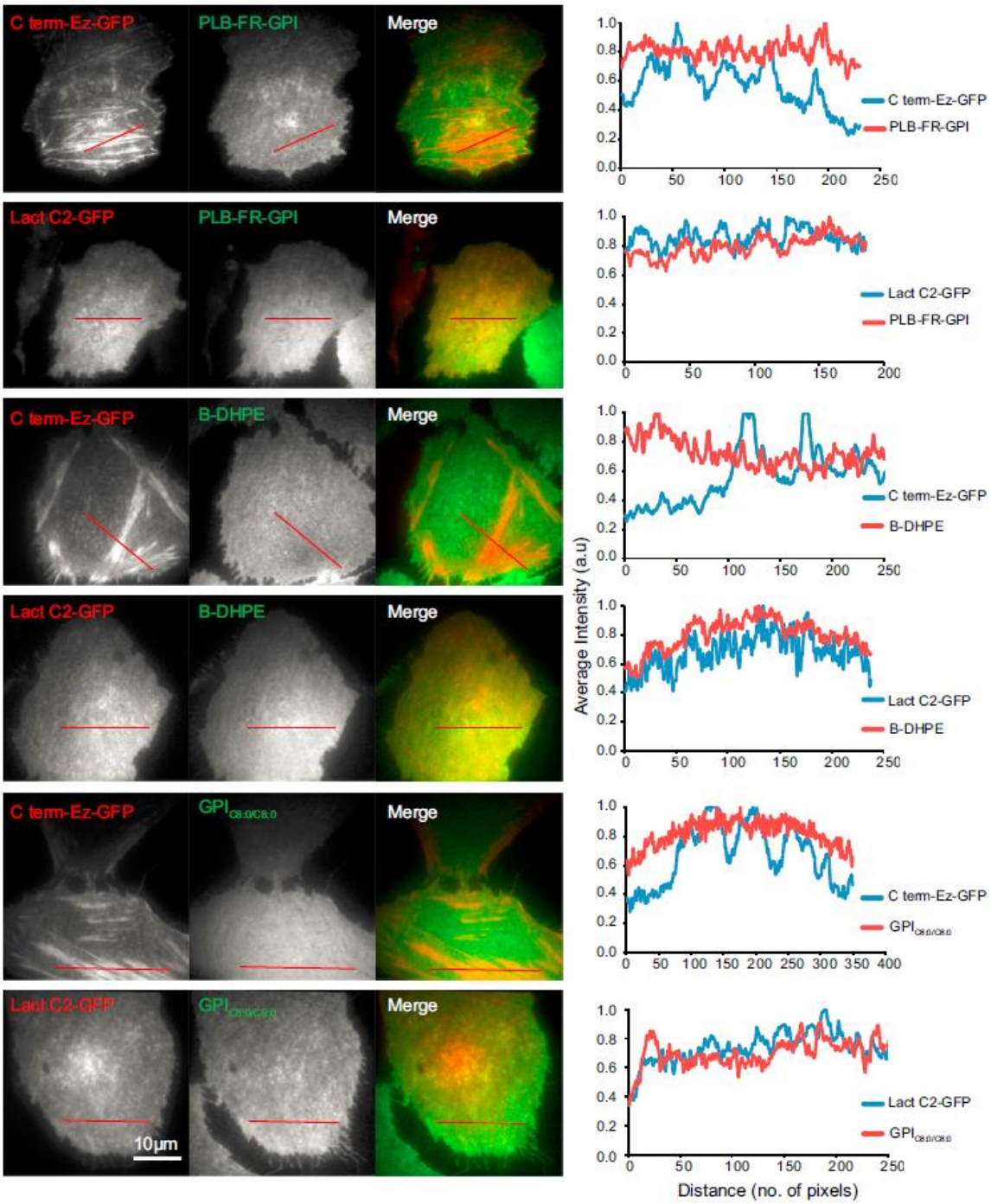

Figure S7. Transbilayer Coupling Exists Only If Either GPI or PS Is Immobilized, Related to Figure 7

Images and line intensity profile of Lact C2 GFP or C-term Ez GFP (ezrin's actin binding domain) transfected in IA2.2 cells labeled with PLB or incorporated with B˙DHPE or $GPI_{C8:0/C8:0}$ as indicated. The data show no colocalization in the distribution of Lact C2 GFP and C term Ez GFP with FR-GPI, Bodipy^{TMR}DHPE and $GPI_{C8:0/C8:0}$ indicating lack of communication across the bilayer in the absence of any physical connection between GPI and PS as represented in Figure 7. Red line in panel D depicts the region of line scan measurement. Scale bar, 10μm.